Solid State Ionics 320 (2018) 378–386

Contents lists available at ScienceDirect

Solid State Ionics

journal homepage: www.elsevier.com/locate/ssi

# Thermal stability of 5 V $LiCoMnO_4$ spinels with LiF additive

Anna Windmüller[a,b,*], Christian Dellen[a,b], Sandra Lobe[a,b], Chih-Long Tsai[a,b], Sören Möller[a,b], Yoo Jung Sohn[a,b], Nadine Wettengl[c], Martin Finsterbusch[a,b], Sven Uhlenbruck[a,b], Olivier Guillon[a,b]

[a] Forschungszentrum Jülich GmbH, Institute of Energy and Climate Research (IEK-1), 52425 Jülich, Germany
[b] Jülich Aachen Research Alliance: JARA-Energy, 52425 Jülich, Germany
[c] Forschungszentrum Jülich GmbH, Central Institute for Engineering, Electronics and Analytics (ZEA-3), 52425 Jülich, Germany

ARTICLE INFO

*Keywords:*
$LiCoMnO_4$ spinel
LiF additive
Thermal stability

ABSTRACT

The thermal stability of $LiCoMnO_4$ and $LiCoMnO_4$ with 1 wt.-% LiF as an additive was compared upon heating in air. The stoichiometries of samples heat-treated at 700, 800, 900 and 1000 °C were analyzed by means of inductively coupled plasma optical emission spectroscopy for cation contents, inert gas fusion analysis for oxygen, and nuclear reaction analysis for fluorine contents, revealing that the sample chemistries remain constant except for oxygen. The oxygen content of the samples correlates with the $Li_2MnO_3$ secondary phase fraction, which forms upon heating, as is shown by X-ray powder diffraction. For each temperature, a greater amount of $Li_2MnO_3$ is formed in the samples with LiF addition than in the single $LiCoMnO_4$ samples. In situ high-temperature X-ray powder diffraction between 650 and 950 °C demonstrates that $LiCoMnO_4$ with LiF addition exhibits the same kind of decomposition reactions upon heating and cooling as the sample without LiF addition. However, for the samples with LiF addition, the formation of the decomposition product, $Li_2MnO_3$, is accelerated due to the excess Li through LiF addition, i.e. the stability of the spinel phase decreases due to the supply of lithium. Since lithium is consumed by $Li_2MnO_3$ formation and fluorine remains in the samples, we can also conclude that the fluorine anion is incorporated into the spinel or $Li_2MnO_3$ phase upon heating $LiCoMnO_4$ and LiF together.

## 1. Introduction

Secondary lithium-ion batteries today offer the highest energy density of all state-of-the-art rechargeable battery systems, which is why they are the most popular energy storage systems for portable electronic devices. In order to meet the requirements of future energy technologies, such as in the field of electric mobility, even higher energy densities are required. Spinel cathodes based on a $LiMn_2O_4$ spinel with nickel, cobalt, or iron substitutions for manganese allow for higher energy densities than the standard cathodes due to their high redox potentials [1,2]. $LiCoMnO_4$ has the highest potential among the high-voltage spinels and offers around a 30% greater energy density than conventional $LiCoO_2$ or $LiMn_2O_4$ spinel cathodes [1]. Theoretically, the full capacity of $LiCoMnO_4$ (equivalent to 1 mol lithium) can be extracted at 5–5.2 V vs. $Li/Li^+$, which is the potential of the $Co^{3+/4+}$ redox couple [3].

However, electrochemical experiments show that $LiCoMnO_4$ cathodes suffer from low capacities, low cycling stabilities, and cell degradation [4–8]. To improve the cycling stability and reversible capacity, fluorination with up to 0.1 mol fluorine per formula unit was shown to be effective for $LiCoMnO_4$ [8]. Similarly, several studies reported that fluorination (~0.1 mol per formula unit) of the $LiNi_{0.5}Mn_{1.5}O_4$ high-voltage spinel leads to improved cycling stabilities [9–13] and discharge capacities [9,11]. If fluorination is not performed via post-synthesis at relatively low temperatures (400 to 500 °C) using $NH_4HF_2$ [10,14,15] or fluorine-enriched atmospheres [12], LiF is usually used as a fluorine source for fluorination at higher temperatures (700 to 900 °C) [9,11,13]. Nevertheless, it is still disputed whether fluorination via LiF can be successfully performed at these high temperatures: Luo et al. used LiF to fluorinate a $LiNi_{0.5}Mn_{1.5}O_4$ spinel and demonstrated that fluorine is lost from the sample at 800 °C [16]. For $LiCoMnO_4$ fluorinated with LiF at 800 °C, however, it was shown that fluorine remains in the sample and the fluorine anion is incorporated into the spinel anionic lattice [8]. Similarly, fluorination with LiF at 700 to 800 °C was reported for $LiNi_{0.5}Mn_{1.5}O_4$ [9,11,13,17].

LiF might not only be considered solely as a fluorine source for fluorination but also as a sintering additive to densify $LiCoMnO_4$ spinels if they need to be integrated into future solid-state batteries as

* Corresponding author at: Forschungszentrum Jülich GmbH, 52425 Jülich, Germany.
*E-mail address:* a.windmueller@fz-juelich.de (A. Windmüller).

https://doi.org/10.1016/j.ssi.2018.03.026
Received 22 December 2017; Received in revised form 9 March 2018; Accepted 23 March 2018
Available online 30 March 2018

cathodes. Solid-state batteries [18,19] using a solid electrolyte with a stability of up to 5.5 V vs. $Li/Li^+$ [20] could overcome the problems caused by the use of conventional liquid electrolytes, which decompose at potentials higher than 4.7 V vs. $Li/Li^+$ [21] and result in the degradation of the $LiCoMnO_4$ cells. However, the integration of a cathode into a solid-state battery creates new requirements for the cathode active material itself [22]. One such requirement is that the active material must be tightly bonded and densified to provide lithium ion and electronic diffusion pathways throughout the cathode layer [18]. Bonding and densification can be achieved via sintering. The use of LiF as a sintering additive might thus be helpful to keep processing temperatures low and achieve high densities.

LiF has been used as an effective sintering additive for several oxide class materials, such as perovskites and spinels [23–27]. LiF is known to melt at 845 °C [28] and sintering can be achieved via liquid phase sintering [24,26]. By using LiF as a sintering additive, it was possible to reduce sintering temperatures significantly – from 1400 to 1200 °C for the $MgAl_2O_4$ spinel [27] and from 1700 °C to 1400 °C for $Ba(Ce,Zr)_2O_3$ perovskites [25]. Only very small amounts of LiF are typically required: up to 1 wt.-% for spinels [24,27] or up to 7 wt.-% for perovskites [25]. Usually, the fluorine anion is purposely evaporated from the sample system during sintering or during a post-sintering heat treatment [24,25].

Whether considering LiF as a fluorinating agent or a sintering additive for $LiCoMnO_4$, raises the question what reactions occur between $LiCoMnO_4$ and LiF during heating and how the thermal stability of the $LiCoMnO_4$ is affected. In general, lithium manganese spinels are known to undergo several decomposition reactions upon heating in air, meaning the thermal stability is rather low. Thackeray et al. showed that $LiMn_2O_4$ starts to lose oxygen from its lattice at around 780 °C in air [29]. For $LiCoMnO_4$ in air, oxygen loss was reported by Reeves et al. at even lower temperatures of around 650 °C [30]. The oxygen loss continues upon further heating. In total, 25% of the initial oxygen is lost up until 1000 °C, while the spinel is transformed to a rocksalt-type phase with a cation to oxygen ratio of 1:1 [29,31]. The transformation to the rocksalt phase was reported as occurring via an intermediate phase, which is monoclinic $Li_2MnO_3$ [29,31–33]. After the spinel becomes instable due to the loss of oxygen, $Li_2MnO_3$ forms and coexists with a lithium- and manganese-depleted spinel. Upon further heating, the depleted spinel and $Li_2MnO_3$ react to the rocksalt phase, which starts at 915 °C for $LiMn_2O_4$ [29] and between 850 and 900 °C for Co-substituted spinels, such as $LiCoMnO_4$ [31]. During cooling, oxygen is taken up again and the reactions are reversed, meaning the rocksalt phase separates into $Li_2MnO_3$ and a lithium- and manganese-depleted spinel. Upon further oxygen uptake, $Li_2MnO_3$ and depleted spinel re-homogenize and restore the initial spinel [31,32].

LiF addition would inevitably only bring fluorine as a new component into the system, while lithium is added in excess. However, the thermal stability of $LiMn_2O_4$ is known to decrease for lithium excess [29,32,34–36], which means that the critical temperature at which $Li_2MnO_3$ is formed decreases for higher lithium stoichiometries [32,34]. Furthermore, substituents such as Ni, Co, and Mg reduce the critical stability temperature further [34]. Fluorination at 800 °C, on the other hand, led to an enhanced phase stability of $LiCoMnO_4$ spinels and a reduced fraction of $Li_2MnO_3$ [8].

In this study, we investigate the stability of $LiCoMnO_4$ with 1 wt.-% of LiF as an additive upon heating systematically. X-ray powder diffraction after sample heat treatment and the chemical analysis of cation and anion contents should provide an insight into the phase compositions and chemistries of $LiCoMnO_4$ samples with and without fluorine addition at temperatures ranging from 700 to 1000 °C. Furthermore, in situ high-temperature X-ray powder diffraction should offer an insight into the phase evolution upon heating and cooling to monitor the decomposition reactions of $LiCoMnO_4$ with and without fluorine addition from room temperature up to 950 °C.

## 2. Experimental methods

### 2.1. Synthesis

In order to synthesize $LiCoMnO_4$ spinel powder, the metal nitrates $LiNO_3$ (99%, Sigma Aldrich), $Co(NO_3)_2{\cdot}6H_2O$ (99–101%, Sigma Aldrich), and $Mn(NO_3)_2$ $4H_2O$ (98%, Sigma Aldrich) were weighed according to the desired cation stoichiometry of Li:Co:Mn = 1:1:1 and dissolved in distilled water in a quartz glass beaker. Citric acid was then added to the solution in a molar ratio of $n_{citric\ acid}/n_{cations} = 2$ and stirred until clear solutions were obtained. As a next step, 55 wt.-% of ethylene glycol (relative to citric acid) was added to each solution. The solutions were then stirred continuously and solvents evaporated by increasing the temperature slowly to 300 °C. Subsequently, the precursors were calcined and annealed to obtain the desired phases. The calcination was performed in two steps: the first calcination step was completed after 300 °C for 10 h and 650 °C for 5 h in an open-top furnace; the second step was completed after a further 5 h at 650 °C in a muffle furnace. The sample was then ball-milled in ethanol using yttria-stabilized zirconia balls for homogenization and heat-treated again at 650 °C in alumina crucibles. The as-prepared sample, known as LCMO powder, was mixed with 1 wt.-% LiF using a pestle and mortar to produce LCMOLiF powder.

LCMO and LCMOLiF powders were subjected to heat treatment processes in air in alumina crucibles with lids in muffle furnaces at 700, 800, 900 and 1000 °C for 4, 3, 2, and 2 h, respectively. The heating and cooling rates were 5 K/min. Prior to the heat treatments, the powders were pressed into pellets at a pressure of 370 MPa using pressing dies with a diameter of 13 mm. The densification via pressing assures intimate contact in between the particles and therefore allows for any solid-state reactions that might arise between $LiCoMnO_4$ and LiF.

### 2.2. Phase analysis and chemical analysis

To investigate product phases of the heat-treated LCMO and LCMOLiF samples, X-ray powder diffraction (XRD) was performed using a D4 ENDEAVOR (Bruker AXS) with Cu-$K_\alpha$ radiation. An interval of 10–80°2θ was measured, employing a step width of 0.02°2θ and a 0.75 s/step scan time. Phase analysis was carried out based on the powder diffraction file (PDF) database and the inorganic crystal structure database (ICSD) using the EVA software package (Bruker AXS).

Inductively coupled plasma optical emission spectroscopy (ICP-OES) was performed after sample dilution to quantify cation contents for the LCMO and LCMOLiF samples heat-treated at different temperatures. The samples were diluted in a ratio of 1:20 for the measurements with a Thermo Scientific iCAP 7600 dual-view spectrometer. External calibration was performed using standards prepared by the dilution of Merck Certipur certified plasma emission standards with diluted acids. The measurements were performed using a radio frequency power of 1150 W and a cool gas flow of 12 $l{\cdot}min^{-1}$, auxiliary gas flow of 0.5 $l{\cdot}min^{-1}$, and nebulizer gas flow of 0.55 $l\,min^{-1}$ for 10 s. Each digestion was measured twice and the mean result of three emission lines per element was used for quantification.

Oxygen contents were measured for the heat-treated LCMO and LCMOLiF samples by means of inert gas fusion analysis (IFA) using a LECO TCH-600 analyzer (Leco Corporation, USA) with an infrared detection cell. Five replicates of approx. 14 mg each were weighed and folded into tin capsules (Leco 501-059), placed in nickel baskets (Leco 502-344), and extracted in graphite crucibles in current control mode for 50 s at 920 A. The instrument was calibrated with 10–25 mg pure $ZrO_2$ (Alfa Aesar Puratronic) before the measurements were performed.

The fluorine content of LCMOLiF pellets heat-treated at 700 °C and 1000 °C was determined by nuclear reaction analysis (NRA). The principle of the NRA method is based on the nuclear reactions between a specimen and a proton beam. The proton beam, which is accelerated to the sample causes a nuclear reaction of the fluorine core and a proton

to an instable $^{20}$Ne isotope, which decays to the stable $^{16}$O isotope and an alpha particle. Hence, the determination of fluorine is gained by the analysis of the alpha particle spectrum. The quantification of elements is not limited to fluorine alone and can also be used to quantify lithium and fluorine from the LiF source simultaneously [25] or whole sample chemistries and depth profiles [37]. For the measurements of the samples in this study, the pellets were mounted on a sample holder and installed in the proton beam path. A proton beam of 3 mm in diameter was generated from a tandetron accelerator with a beam energy of 3.24 MeV. A 50 mm$^2$ passivated implanted planar silicon detector with a sensitive thickness of 300 µm was installed in backscattering geometry at 165° and at a distance of 100 mm. To guarantee a sufficient signal to noise ratio and resolution, the pile-up contribution (distortion by pulse overlap) was kept at less than 10% by setting the proton current to ~10 nA. The collected charge was around 100 µC for each measurement. Cross-section data from Ranken et al. [38] were used to fit the experimental results with the SIMNRA 6.06 software [39]. The cross sections of fluorine were verified using a LiF sample for calibration prior to the measurements.

### 2.3. In situ high-temperature X-ray powder diffraction

The phase evolution during heating was further investigated by means of in situ high-temperature XRD in ambient air using an Empyrean (PANalytical B.V.) with Cu-K$_\alpha$ radiation. Samples of LCMO powder were prepared in an alumina front-loading sample holder. Another sample of LCMOLiF powder was pelletized. For the pelletizing process, the powder was pressed at a pressure of 370 MPa using a pressing die with a diameter of 20 mm and was mounted onto an alumina sample holder. Diffractograms were collected at room temperature before and after each in situ measurement. The in situ measurements were performed for isotherms at selected temperatures from 650 °C to 950 °C and back to 650 °C with a step size of 50 K/step. For each temperature, 5 scans were collected from 15 to 64°2θ. The total holding time at each temperature was 34 min. The heating ramps between the steps were 5 K/min, where no scan was performed. After careful examination of the five individual scans at each temperature (Fig. S2), the five scans were averaged to produce a representative scan for each temperature with an improved signal to noise ratio. The averaged scans were used for the quantification of phase fractions and lattice parameters by means of Rietveld analysis within the software package Topas 4 (Bruker AXS) [40].

## 3. Results and discussion

Fig. 1 provides a comparison of the XRD patterns for the LCMO and LCMOLiF samples after heat treatment at different temperatures. A $LiCoMnO_4$ spinel, with a = 8.06 Å [2], can be identified in all eight samples. In addition, monoclinic $Li_2MnO_3$ (space group *C2/m*), which was already present in the pristine powder (Fig. S1), is identified from its (*001*) and (*020*) reflections [41]. Since the $LiCoMnO_4$ spinel and the monoclinic $Li_2MnO_3$ phase are structurally related, most of the $Li_2MnO_3$ Bragg peaks overlap with the spinel Bragg peaks.

The intensities of the (*001*) and (*020*) reflections of the $Li_2MnO_3$ phase increase with rising temperatures for both samples, and shoulders appear for the peaks at higher diffraction angles, where peak overlap of spinel and $Li_2MnO_3$ predominantly occurs. This observation indicates higher phase fractions of the $Li_2MnO_3$ phase for samples heat-treated at a higher temperature. A further comparison of the LCMO and LCMOLiF diffraction patterns for the samples heat-treated at 900 °C points to higher fractions of the $Li_2MnO_3$ phase in the LCMOLiF sample. This is visible through the higher intensity of the (*001*) and (*020*) reflections in the LCMOLiF diffraction pattern and the shoulders appearing at higher diffraction angles, which are caused by overlapped diffraction peaks of the $Li_2MnO_3$ phase. Furthermore, the spinel peaks shift to lower diffraction angles when the applied temperature increases. For the

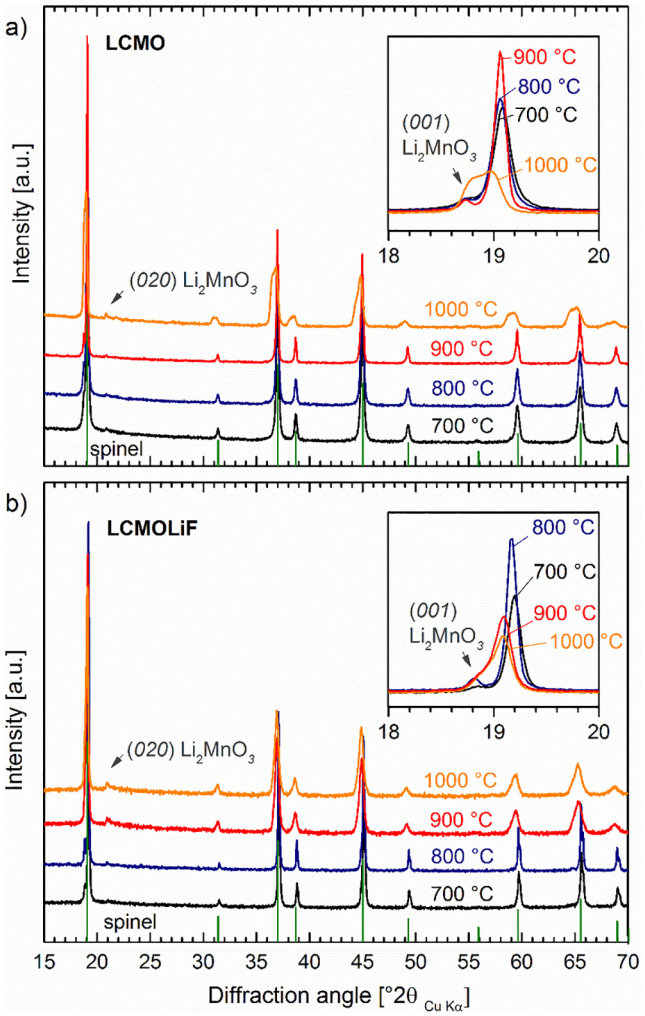


**Fig. 1.** Results of ex situ XRD on a) LCMO and b) LCMOLiF samples after heat treatment at different temperatures. The vertical lines refer to the Bragg positions of the spinel phase [2].

LCMOLiF samples, this peak shift is stronger than for the LCMO samples. This means that a significant peak shift to lower diffraction angles is observed for the spinel phase in the LCMO sample heat-treated at 1000 °C, whereas for the LCMOLiF samples, a clear shift is already apparent for the samples heat-treated at 900 °C.

These results suggest that LiF addition already has a major impact on the phase stability of the $LiCoMnO_4$ spinel at higher temperatures. The peak shifts to lower angles indicate a widening of the lattice due to a change in the spinel stoichiometry. The change in stoichiometry might be a result of the lithium and manganese depletion of the spinel phase upon $Li_2MnO_3$ formation, as was observed for $LiMn_2O_4$ and $LiCoMnO_4$ spinels [29,30]. Besides $Li_2MnO_3$ formation, changes in the overall sample stoichiometry can occur due to evaporating lithium or transition metal fluorides, as was observed in [16,23,25].

In order to monitor changes in the cation stoichiometry of the samples, the LCMO and LCMOLiF samples were analyzed by means of ICP-OES (Fig. 2, Table 1, Table S1). For the samples heat-treated at 700 °C, lithium, manganese, and cobalt contents were quantified to 3.7 ± 0.1 wt.-%, 29.4 ± 0.2 wt.-%, and 31.5 ± 0.2 wt.-% for LCMO, which corresponds to a sample stoichiometry of $LiCoMnO_{3.87}$ (normalized to 3 cations). For LCMOLiF heat-treated at 700 °C they were quantified to 4.3 ± 0.1 wt.-% (Li), 29.2 ± 0.5 wt.-% (Mn) and 31.4 ± 0.5 wt.-% (Co), this corresponds to a sample stoichiometry of $Li_{1.11}Co_{0.95}Mn_{0.95}O_{3.64}$. The additional lithium from the LiF source is reflected in the higher amount of lithium in the LCMOLiF sample

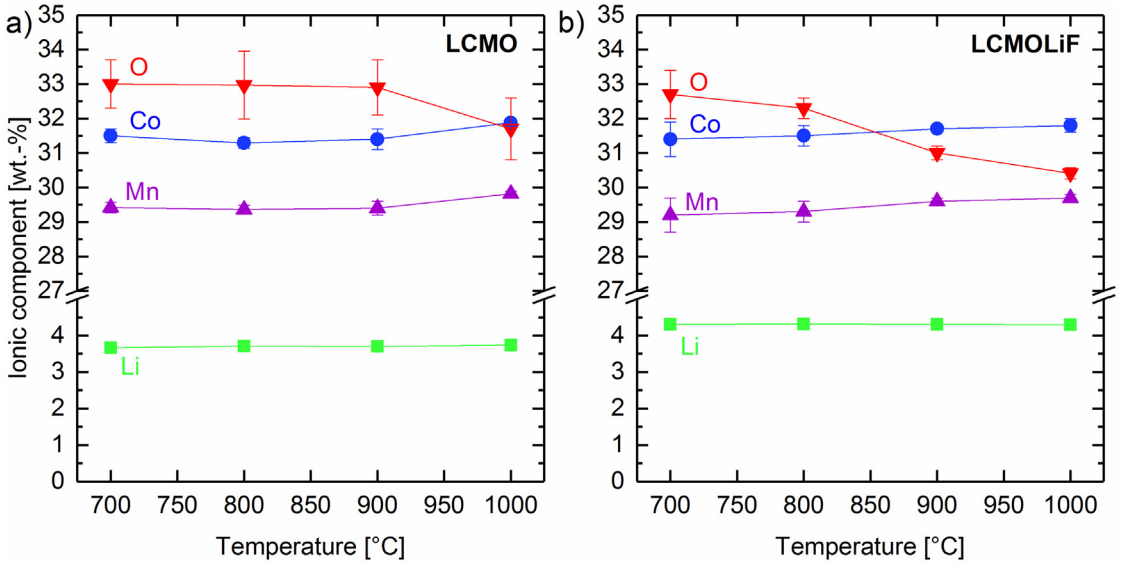


**Fig. 2.** Changes in chemistry for samples a) LCMO and b) LCMOLiF heat-treated at different temperatures.

**Table 1**
Stoichiometry of a) LCMO and b) LCMOLiF samples after heat treatment at different temperatures in mol per formula unit ($LiCoMnO_4$). The mol fractions were calculated from the weight fractions as measured using ICP-OES (for cations) and IFA (for oxygen) by normalizing to 3 cations per formula unit (measured weight fractions are listed in Tables S1 and S2).

a) LCMO

| Temperature [°C] | Li [mol] | Co [mol] | Mn [mol] | O [mol] |
|---|---|---|---|---|
| 700 | 0.99 ± 0.01 | 1.00 ± 0.01 | 1.01 ± 0.01 | 3.87 ± 0.08 |
| 800 | 1.00 ± 0.01 | 1.00 ± 0.01 | 1.00 ± 0.01 | 3.87 ± 0.12 |
| 900 | 1.00 ± 0.02 | 1.00 ± 0.01 | 1.00 ± 0.01 | 3.86 ± 0.09 |
| 1000 | 1.01 ± 0.01 | 1.02 ± 0.01 | 1.02 ± 0.01 | 3.72 ± 0.11 |

b) LCMOLiF

| Temperature [°C] | Li [mol] | Co [mol] | Mn [mol] | O [mol] |
|---|---|---|---|---|
| 700 | 1.11 ± 0.02 | 0.95 ± 0.02 | 0.95 ± 0.02 | 3.64 ± 0.08 |
| 800 | 1.11 ± 0.01 | 0.95 ± 0.01 | 0.95 ± 0.01 | 3.59 ± 0.03 |
| 900 | 1.11 ± 0.01 | 0.96 ± 0.01 | 0.96 ± 0.01 | 3.45 ± 0.02 |
| 1000 | 1.10 ± 0.01 | 0.96 ± 0.01 | 0.96 ± 0.01 | 3.38 ± 0.02 |

compared to the LCMO sample.

Upon heating, the cation weight fractions increase slightly for both sample systems, indicating a loss of total mass at higher temperatures. The lost mass is the result of a loss of oxygen, as can be shown by the quantification of the oxygen stoichiometry by means of IFA. The LCMO samples heat-treated at 700, 800, and 900 °C have the same oxygen content (33.0 ± 0.9 wt.-%), which is reduced for the sample heat-treated at 1000 °C (31.7 ± 0.9 wt.-%). The $LiCoMnO_4$ spinels usually lose oxygen upon heating and (partially) take up oxygen again in a reversible manner during cooling [30]. The similar oxygen contents of the samples heat-treated at 700, 800 and 900 °C indicate that the lost oxygen was taken up reversibly by all samples during cooling and that the original oxygen stoichiometry is restored (Table S2). For the sample heat-treated at 1000 °C, the lost oxygen is not taken up again completely – most likely because the equilibrium condition is not yet achieved.

The LCMOLiF samples exhibit a continuous decrease in oxygen content with increasing temperature. The oxygen content for the sample heat-treated at 700 °C is 32.7 ± 0.7 wt.-%, while the sample heat-treated at 1000 °C has an oxygen content of 30.4 ± 0.2 wt.-%. Here, the continuous decrease in oxygen content with increasing temperatures indicates irreversible reactions upon heating due to LiF addition, which hinders reversible oxygen uptake, as will be discussed further below.

In addition to the loss of oxygen, the loss of fluorine is possible, which is why NRA measurements were performed for the LCMOLiF samples heat-treated at 1000 and 700 °C in comparison. Fig. 3 shows the measured spectra for both samples. In the energy range from 7400 to 8000 keV, the scattering and reactions of fluorine occur, which are not overlapped by the energy ranges for the scattering and reactions of the other elements. The measurements of α-particles, which belong to the $^{19}F(p,\alpha_0)^{16}O$ nuclear reaction, can be seen in the inset of Fig. 3. The occurrence of this nuclear reaction verifies the presence of fluorine in both samples. By fitting the spectrum with SIMNRA, the amount of fluorine was quantified to weight fractions of 0.8 ± 0.1 and 0.9 ± 0.1 wt.-% for the samples heat-treated at 700 and 1000 °C, respectively. This is close to the weighed amount of 0.8 wt.-% fluorine (according to 1 wt.-% LiF).

To conclude, the analysis of the cation and anion stoichiometry of the LCMO and LCMOLiF samples does not indicate any change in cation and fluorine contents for both sample systems when heated at up to 1000 °C. Since cation and fluorine contents do not decrease, the evaporation of lithium or transition metal fluorides, which was observed in other studies [16,23,25], can be excluded. Other than for the perovskites or the $MgAl_2O_4$ spinels, temperatures in this study remained below 1000 °C, which might explain why no evaporation of fluorine is observed. The contradiction with the results of Luo et al., who found that fluorine is lost from the sample at 800 °C, might be explained by the pelletizing of the samples and the closed environment chosen during heat treatment in this study, which might hinder fluorine evaporation. The pelletizing assures a higher density of the sample and allows for a close contact of LiF and spinel particles, which promotes the solid-state reaction of LiF and spinel before LiF starts to vaporize. The only evaporating component is oxygen, which decreased significantly for both sample systems at higher temperatures. The decreasing oxygen stoichiometries are correlated to a higher $Li_2MnO_3$ fraction for the samples heat-treated at higher temperatures.

In order to gain further insight into the evolution of crystalline phases during sintering, an in situ high-temperature XRD study was conducted for LCMO and LCMOLiF samples. Fig. 4 shows the qualitative evolution of phases for the LCMO sample. At 650 °C, the pattern indicates the presence of the $LiCoMnO_4$ spinel and the $Li_2MnO_3$ phase, which is in agreement with the phase content of the as-prepared LCMO powder (Fig. S1).

Upon heating, the spinel peaks exhibit a shift to lower angles,

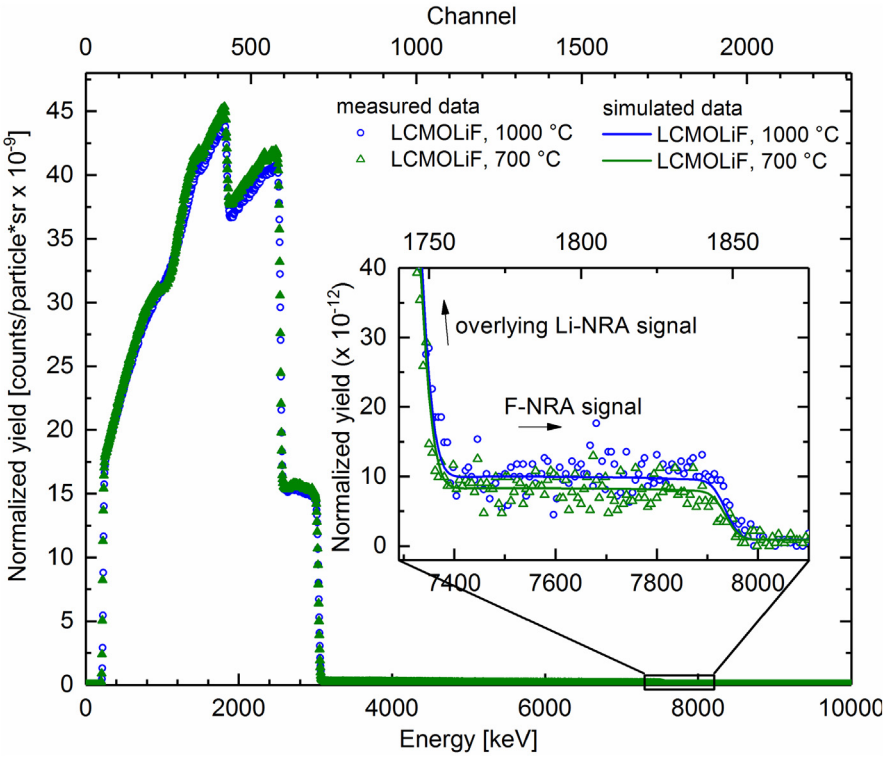


**Fig. 3.** Measured and simulated NRA data for LCMOLiF samples heat-treated at 700 and 1000 °C. The inset shows the non-overlapped NRA data of fluorine. The yield was normalized to the particle*sr factor (= number of incident particles multiplied by the solid angle of the detector).

implying larger lattice parameters at higher temperatures. A thermal expansion of the lattice is expected upon heating. However, the relative intensities of the main spinel reflections also change upon heating. The spinel (*111*) reflection is strongest at 650 °C and continuously fades until 950 °C. The (*311*) refection becomes the main reflection and the (*220*) reflection increases in intensity, as is typical for $(Co,Mn)_3O_4$ spinels [42,43]. This observation indicates a change in the stoichiometry of the spinel phase, i.e. a chemical expansion of the lattice in addition to the thermal expansion. This agrees with the in situ XRD studies on $LiCoMnO_4$ in oxygen atmosphere by Reeves et al. [30] and Pasero et al. [44] and is a result of $Li_2MnO_3$ formation and lithium and manganese depletion of the spinel phase. Consequently, an increase in the $Li_2MnO_3$ fraction is observed from the rising peak intensity of its main reflection at 18.5°2θ, as can be seen in the excerpts from 19 to 20°2θ in Fig. 4.

At 850 °C, no more $Li_2MnO_3$ reflections are identified and a new (Li,Co,Mn)O phase appears in rocksalt configuration (space group *Fm-3 m*). Spinel peaks can still be identified but the intensity ratios of the (*111*) to the (*311*) reflection and the increased intensity of the (*220*) reflection in particular suggest a change in its chemistry to a lithium-depleted $(Co,Mn)_3O_4$ spinel, which is in agreement with [30,44]. At the highest temperature (950 °C), the spinel is still the main phase. During cooling, the reactions are reversed, i.e. the rocksalt phase disappears again and $Li_2MnO_3$ reappears and exhibits increasing intensities of its reflections, while the peaks of $LiCoMnO_4$ return to their original positions. The reversible reaction of $LiMn_2O_4$ or $LiCoMnO_4$ to $LiMn_2O_3$ or $LiCoMnO_3$, respectively, with $Li_2MnO_3$ as an intermediate phase, has been previously described in literature [29,30]. The results here are in good agreement with what has been reported.

For the LCMOLiF sample, the phase evolution is different (Fig. 5). From 650 to 850 °C the spinel peaks exhibit a similar shift and change in relative intensities, as was observed for the LCMO sample. However, the relative intensities of the $Li_2MnO_3$ Bragg reflections are higher at each single temperature than is observed for the LCMO sample at the same temperatures. This observation implies a higher $Li_2MnO_3$ content in the LCMOLiF sample than in the LCMO sample at each given temperature. Furthermore, the spinel peaks disappear for LCMOLiF at 850 °C and 900 °C and the patterns reveal a contribution of the rocksalt-type phase only. Below 850 °C during cooling, the spinel phase is restored and no more peaks of the rocksalt phase are observed.

Quantification of the occurring phases via the Rietveld method allows for a more detailed insight into the phase evolution during heating and cooling for a better comparison of the two sample systems. Changes in the cation chemistry were allowed during the refinements to describe the changing intensity ratios of the spinel and rocksalt reflections. In particular, the transition metal occupancy of the *8a* spinel site was refined as well as the transition metal occupancy of the *4a* site in the rocksalt phase. Tables S3 and S4 provide a detailed overview of the resulting refined parameters, including R-values, transition metal occupancies, and weight fractions of the quantified phases.

Fig. 6 depicts the results of the quantitative phase analysis. The phase fractions in both samples are the same at the beginning of the measurement, at room temperature, which is around 10 wt.-% $Li_2MnO_3$ and 90 wt.-% $LiCoMnO_4$. For LCMO, the $Li_2MnO_3$ fraction remains at around 10 wt.-% at 650 °C. From 650 to 800 °C, this fraction increases from 10 wt.-% to 30 wt.-%, while the fraction of the spinel phase decreases. For temperatures above 800 °C, the rocksalt phase emerges and increases in weight fraction as the temperature increases, while the weight fractions for spinel and $Li_2MnO_3$ decrease. At the maximum temperature of 950 °C, no more $Li_2MnO_3$ is detected, the rocksalt phase is the main phase, and 40 wt.-% of the spinel phase remains. During cooling, the phase evolution displays a completely reversible trend. After the high-temperature measurements, 10 wt.-% $Li_2MnO_3$ and 90 wt.-% $LiCoMnO_4$ are again observed, as revealed by the refinement of the scan at room temperature following the experiment.

The first differences between the LCMO and LCMOLiF samples are already apparent from the phase evolution between 25 °C and 650 °C upon heating. The initial $Li_2MnO_3$ fraction of 10 wt.-% at 25 °C for LCMOLiF is doubled at 650 °C. We know from the literature that $Li_2MnO_3$ formation occurs in the Li–Mn–O ternary system due to

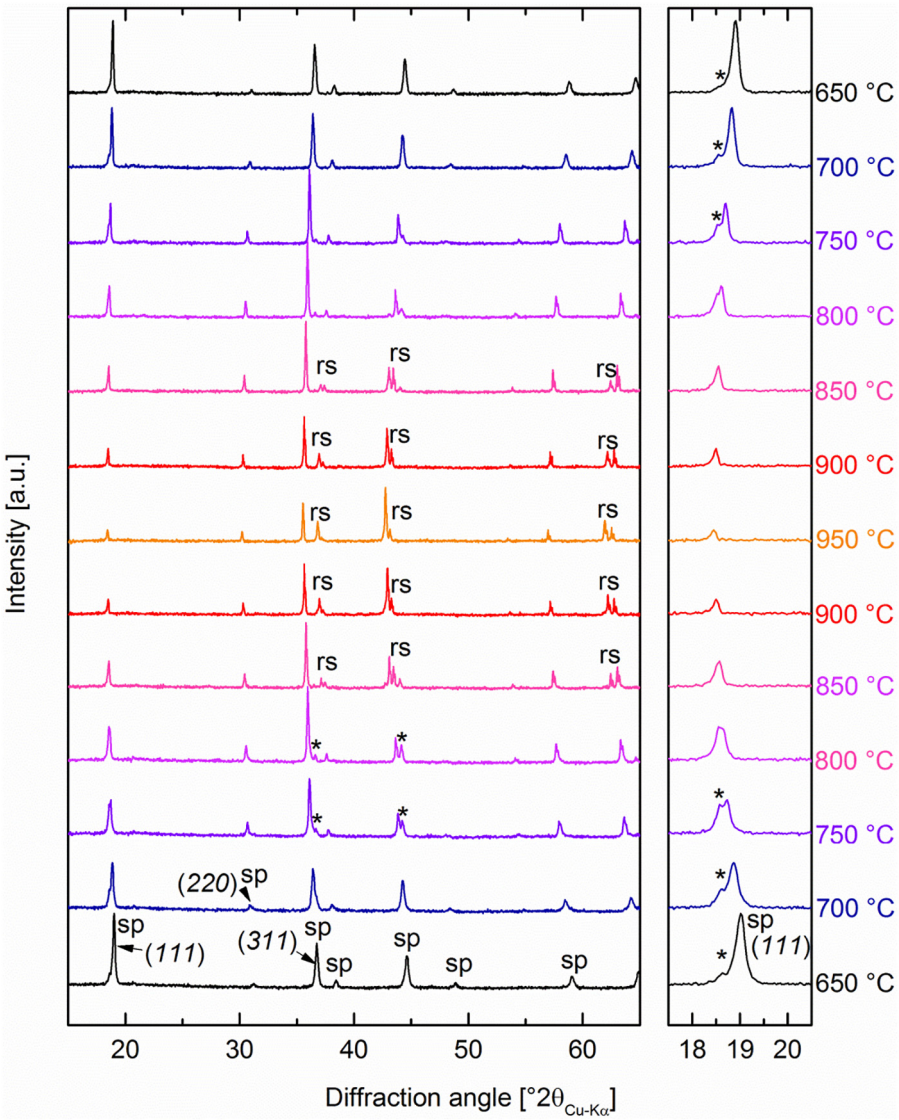


**Fig. 4.** Averaged diffractograms for the in situ high-temperature XRD of LCMO powder for heating from 650 °C to 950 °C and cooling to 650 °C (bottom to top); phase labeling: spinel (sp), $Li_2MnO_3$ (*) and rock-salt (rs).

oxygen loss or lithium supply [29,32,34,36]. In the investigated sample system, LiF appears to act as a lithium source initiating the formation of additional $Li_2MnO_3$ at a temperature of already below 650 °C, leading to an accelerated formation of $Li_2MnO_3$ in the LCMOLiF sample compared to the LCMO sample. The formation of $Li_2MnO_3$ in the LCMOLiF sample at a lower temperature than in the LCMO sample agrees with the studies of Luo and Martin [34] and Cupid et al. [32] on the phase stability of $LiMn_2O_4$ spinel, where it was found that excess Li reduces the thermal stability of the spinel phase and leads to earlier $Li_2MnO_3$ formation.

From 650 °C to 800 °C, the $Li_2MnO_3$ fraction in the LCMOLiF sample further increases to 50 wt.-%, leaving behind 50 wt.-% of spinel phase. In comparison to the LCMO sample at 800 °C, the LCMOLiF sample contains 20 wt.-% more $Li_2MnO_3$. The lithium supply from 1 wt.-% LiF alone (= 5.5 mol.-%) would only allow for additional $Li_2MnO_3$ of ~10 wt.-%. The additional ~10 wt.-% of $Li_2MnO_3$, which is observed at 800 °C for LCMOLiF, can only arise from an accelerated decomposition reaction of spinel, thus supplying lithium for $Li_2MnO_3$ formation. This is again in agreement with the studies of Luo and Martin [34] and Cupid et al. [32], which show how small amounts of excess lithium can significantly reduce the phase stability of spinel: 0.1 mol excess lithium for $LiMn_2O_4$ lowered the critical stability temperature for spinel by 100 °C [32].

Beyond 800 °C, $Li_2MnO_3$ and spinel are known to react to a $LiMnCoO_3$ phase in rocksalt configuration, while oxygen is released from the sample continuously [30]. The reaction of spinel and $Li_2MnO_3$ to the rocksalt-type phase starts at between 800 and 850 °C for both the LCMO and LCMOLiF samples. Due to the higher fraction of $Li_2MnO_3$ in LCMOLiF below 800 °C, the resulting fraction of the rocksalt phase is much higher than in the LCMO sample (90 wt.-% vs. 30 wt.-% at 850 °C). At 900 °C, the rocksalt phase is the only phase detected by XRD in the LCMOLiF sample. The reaction of $Li_2MnO_3$ and spinel to rocksalt between 800 and 850 °C agrees with the studies of Reeves et al. where the rocksalt phase first emerged in samples quenched from 850 °C.

The phase evolution is reversed upon cooling for both samples, i.e. the rocksalt phase separates completely into spinel and $Li_2MnO_3$, which agrees with the studies on the reversible reactions of $LiMn_2O_4$ and $LiCoMnO_4$ in air [29–31]. While the reaction is completely reversible for LCMO, the LCMOLiF samples only exhibit a partially reversible reaction. This means that at 25 °C, 15 wt.-% $Li_2MnO_3$ is detected, which is 5 percentage points higher than the initial fraction. The lithium brought into the system by LiF is therefore completely consumed by $Li_2MnO_3$ formation. This result again agrees with the phase diagrams of Luo and Martin [34] and Cupid et al. [32], who reported that the phase stability

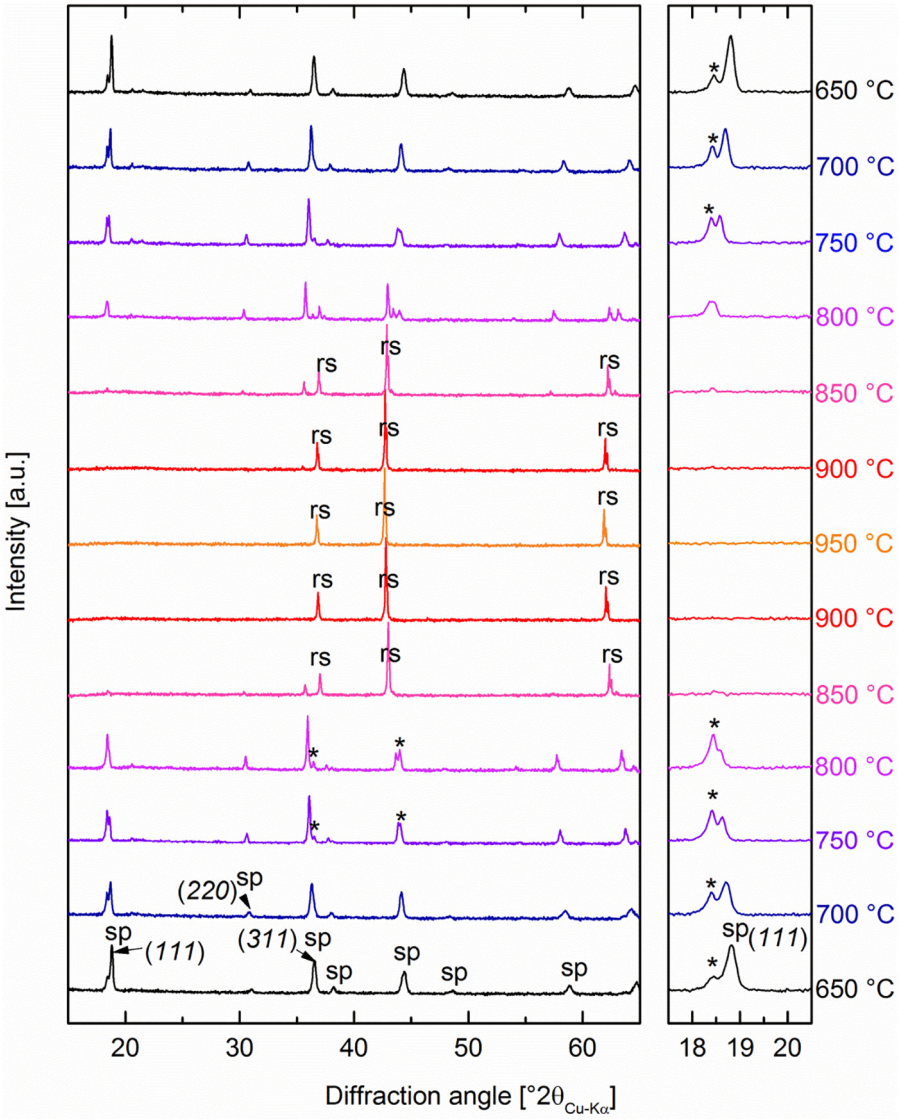


**Fig. 5.** Averaged diffractograms from the in situ high-temperature XRD of the LCMOLiF pellet for heating from 650 °C to 950 °C and cooling to 650 °C (bottom to top); phase labeling: spinel (sp), $Li_2MnO_3$ (*) and rock-salt (rs).

of spinel is reduced for excess lithium and that more $Li_2MnO_3$ is formed.

To summarize the results from the in situ high-temperature XRD, LiF accelerates the formation of $Li_2MnO_3$ at a temperature of already below 650 °C through the additional supply of lithium. This leads to an extended depletion of spinel and accelerated formation of $Li_2MnO_3$ between 650 °C and 800 °C as well as the extended formation of $LiCoMnO_3$ above 800 °C. The reactions of $Li_2MnO_3$ and spinel to $LiCoMnO_3$ are completely reversible, as is the case for the sample without LiF addition. However, the content of $Li_2MnO_3$ in the LCMOLiF sample is higher after the in situ high-temperature XRD measurement than it was before. This is a result of the reduced stability of the spinel phase, i.e. the formation of $Li_2MnO_3$ due to the supply of Li from the LiF source, which occurs at below 650 °C.

Since lithium from the LiF source is consumed by $Li_2MnO_3$ formation and fluorine remains within the samples at higher temperatures, we can conclude that the fluorine anion is most likely incorporated into the lattice of spinel and/or the secondary phases. The incorporation of fluorine into either $Li_2MnO_3$ or lithium manganese spinels has been reported in several studies [9,16,45,46]. For the $LiCoMnO_4$ spinel in particular, it was shown that fluorination has a positive impact on the electrochemical performance of the spinel due to a stabilizing effect on the spinel lattice [8].

## 4. Conclusion

The addition of 1 wt.-% LiF to $LiCoMnO_4$ leads to extended $Li_2MnO_3$ formation in the Li–Co–Mn–O system and a reduced stability of the spinel phase. All lithium from the LiF source was consumed by $Li_2MnO_3$ formation. The evaporation of any fluorine species, such as transition metal fluorides, was shown to be false. The results strongly suggest that the fluorine anion from the LiF source is incorporated into the spinel and/or secondary phases during the thermal reaction of LiF with $LiCoMnO_4$.

## Acknowledgements

We would like to thank the Helmholtz Association of German Research Centres (PoF3-SCI) for financial support as part of the “Speicher und vernetzte Infrastrukturen” grant and from the German Federal Ministry of Education and Research as part of the DESIREE project (project no. 03SF0477A).

The authors would also like to thank Karin Lühring, Forschungszentrum Jülich, Central Institute of Engineering, Electronics and Analytics – Analytics (ZEA-3), for oxygen quantification.

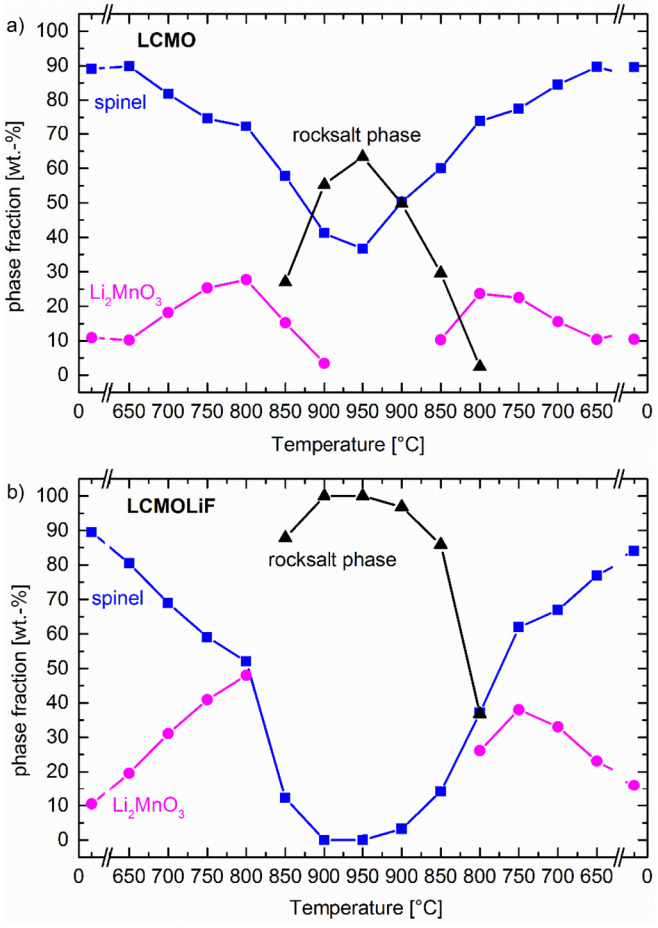


**Fig. 6.** Quantification of phases from the in situ high-temperature XRD data: a) LCMO sample, b) LCMOLiF sample.

## Appendix A. Supplementary data

Supplementary data to this article can be found online at https://doi.org/10.1016/j.ssi.2018.03.026.

## References


[1] M.S. Whittingham, Lithium batteries and cathode materials, Chem. Rev. 104 (2004) 4271–4302.
[2] H. Kawai, M. Nagata, H. Tukamoto, A.R. West, High-voltage lithium cathode materials, J. Power Sources 81–82 (1999) 67–72.
[3] H. Kawai, M. Nagata, H. Tukamoto, A.R. Westa, A. New Lithium, Cathode $LiCoMnO_4$: toward practical 5 V lithium batteries, Electrochem. Solid-State Lett. 1 (1998) 212–214.
[4] M. Hu, Y. Tian, J. Wei, D. Wang, Z. Zhou, Porous hollow $LiCoMnO_4$ microspheres as cathode materials for 5 V lithium ion batteries, J. Power Sources 247 (2014) 794–798.
[5] J.M. Amarilla, R.M. Rojas, F. Pico, L. Pascual, K. Petrov, D. Kovacheva, M.G. Lazarraga, I. Lejona, J.M. Rojo, Nanosized $LiMYMn_2-YO_4$ (M = Cr, Co and Ni) spinels synthesized by a sucrose-aided combustion method: Structural characterization and electrochemical properties, 13th International Meeting on Lithium Batteries, 174 2007, pp. 1212–1217.
[6] H. Shigemura, M. Tabuchi, H. Kobayashi, H. Sakaebe, A. Hirano, H. Kageyama, Structural and electrochemical properties of Li(Fe,Co)x$Mn_2$-x$O_4$ solid solution as 5 V positive electrode materials for Li secondary batteries, J. Mater. Chem. 12 (2002) 1882–1891.
[7] R. Alcantara, M. Jaraba, P. Lavela, J.L. Tirado, Electrochemical, 6Li MAS NMR, and X-ray and Neutron Diffraction Study of LiCoxFeyMn$_2$-(x + y)$O_4$ Spinel Oxides for High-Voltage Cathode Materials, Chem. Mater. 15 (2003) 1210–1216.
[8] A. Windmüller, C.-L. Tsai, S. Möller, M. Balski, Y.J. Sohn, S. Uhlenbruck, O. Guillon, Enhancing the performance of high-voltage $LiCoMnO_4$ spinel electrodes by fluorination, J. Power Sources 341 (2017) 122–129.
[9] N.M. Hagh, G.G. Amatucci, Effect of cation and anion doping on microstructure and electrochemical properties of the $LiMn_{1.5}Ni_{0.5}O_4-\delta$ spinel, J. Power Sources 256 (2014) 457–469.
[10] W. Choi, A. Manthiram, Superior capacity retention spinel oxyfluoride cathodes for lithium-ion batteries, Electrochem. Solid-State Lett. 9 (2006) A245–A248.
[11] H. Li, Y. Luo, J. Xie, Q. Zhang, L. Yan, Effect of lithium and fluorine doping on the electrochemical and thermal stability of $LiNi_{0.5}Mn_{1.5}O_4$ spinel cathode material, J. Alloys Compd. 639 (2015) 346–351.
[12] A. Höweling, D. Stenzel, H. Gesswein, M. Kaus, S. Indris, T. Bergfeldt, J.R. Binder, Variations in structure and electrochemistry of iron- and titanium-doped lithium nickel manganese oxyfluoride spinels, J. Power Sources 315 (2016) 269–276.
[13] G. Du, Y. NuLi, J. Yang, J. Wang, Fluorine-doped $LiNi_{0.5}Mn_{1.5}O_4$ for 5 V cathode materials of lithium-ion battery, Mater. Res. Bull. 43 (2008) 3607–3613.
[14] T. Okumura, T. Fukutsuka, K. Matsumoto, Y. Orikasa, H. Arai, Z. Ogumi, Y. Uchimoto, Role of local and electronic structural changes with partially anion substitution lithium manganese spinel oxides on their electrochemical properties: X-ray absorption spectroscopy study, Dalton Trans. 40 (2011) 9752–9764.
[15] K. Matsumoto, T. Fukutsuka, T. Okumura, Y. Uchimoto, K. Amezawa, M. Inaba, A. Tasaka, Electronic structures of partially fluorinated lithium manganese spinel oxides and their electrochemical properties, Selected Papers Presented at the 14th INTERNATIONAL MEETING ON LITHIUM BATTERIES (IMLB-2008), 189 2009, pp. 599–601.
[16] Q. Luo, T. Muraliganth, A. Manthiram, On the incorporation of fluorine into the manganese spinel cathode lattice, Solid State Ionics 180 (2009) 703–707.
[17] S.-W. Oh, S.-H. Park, J.-H. Kim, Y.C. Bae, Y.-K. Sun, Improvement of electrochemical properties of $LiNi_{0.5}Mn_{1.5}O_4$ spinel material by fluorine substitution, J. Power Sources 157 (2006) 464–470.
[18] S. Uhlenbruck, J. Dornseiffer, S. Lobe, C. Dellen, C.-L. Tsai, B. Gotzen, D. Sebold, M. Finsterbusch, O. Guillon, Cathode-electrolyte material interactions during manufacturing of inorganic solid-state lithium batteries, J. Electroceram. (2016) 1–10.
[19] J. Li, C. Ma, M. Chi, C. Liang, N.J. Dudney, Solid Electrolyte, Adv. Energy Mater. 5 (2015) (n/a-n/a).
[20] C.-L. Tsai, E. Dashjav, E.-M. Hammer, M. Finsterbusch, F. Tietz, S. Uhlenbruck, H.P. Buchkremer, High conductivity of mixed phase Al-substituted $Li_7La_3Zr_2O_{12}$, J. Electroceram. 35 (2015) 25–32.
[21] W. Xu, X. Chen, F. Ding, J. Xiao, D. Wang, A. Pan, J. Zheng, X.S. Li, A.B. Padmaperuma, J.-G. Zhang, Reinvestigation on the state-of-the-art nonaqueous carbonate electrolytes for 5 V Li-ion battery applications, J. Power Sources 213 (2012) 304–316.
[22] T. Placke, R. Kloepsch, S. Dühnen, M. Winter, Lithium ion, lithium metal, and alternative rechargeable battery technologies: the odyssey for high energy density, J. Solid State Electrochem. 21 (2017) 1939–1964.
[23] M. Du Rubat Merac, I.E. Reimanis, H.-J. Kleebe, Electrochemical impedance spectroscopy of transparent polycrystalline magnesium aluminate ($MgAl_2O_4$) spinel, J. Am. Ceram. Soc. 98 (2015) 2130–2138.
[24] I.E. Reimanis, H.-J. Kleebe, Reactions in the sintering of $MgAl_2O_4$ spinel doped with LiF, IJMR 98 (2007) 1273–1278.
[25] C.-L. Tsai, M. Kopczyk, R.J. Smith, V.H. Schmidt, Low temperature sintering of Ba$(Zr_{0.8-x}Ce_xY_{0.2})O_{3-\delta}$ using lithium fluoride additive, Solid State Ionics 181 (2010) 1083–1090.
[26] M. Pollet, S. Marinel, Low temperature sintering of $CaZrO_3$ using lithium fluoride addition, J. Eur. Ceram. Soc. 23 (2003) 1925–1933.
[27] K. Rozenburg, I.E. Reimanis, H.-J. Kleebe, R.L. Cook, sintering kinetics of a $MgAl_2O_4$ spinel doped with LiF, J. Am. Ceram. Soc. 91 (2008) 444–450.
[28] D.R. Lide, CRC Handbook of Chemistry and Physics, 2005–2006 CRC Press, Taylor & Francis, Boca Raton, FL, 2005.
[29] M.M. Thackeray, M.F. Mansuetto, D.W. Dees, D.R. Vissers, The thermal stability of lithium-manganese-oxide spinel phases, Mater. Res. Bull. 31 (1996) 133–140.
[30] N. Reeves, C.A. Kirk, A.R. West, Reversible spinel to rock salt transition in $LiCoMnO_{4-\delta}$ by oxygen (de) intercalation, J. Mater. Chem. 11 (2001) 249–250.
[31] N. Reeves-McLaren, J. Sharp, H. Beltran-Mir, W.M. Rainforth, A.R. West, Spinel-rock salt transformation in $LiCoMnO_{4-d}$, Proc. R. Soc. A 472 (2016) 20140991.
[32] D.M. Cupid, T. Lehmann, T. Bergfeldt, H. Berndt, H.J. Seifert, Investigation of the lithium-rich boundary of the $Li_{1+x}Mn_{2-x}O_4$ cubic spinel phase in air, J. Mater. Sci. 48 (2013) 3395–3403.
[33] D. Pasero, N. Reeves, V. Pralong, A.R. West, Oxygen nonstoichiometry and phase transitions in $LiMn_{1.5}Ni_{0.5}O_{4-\delta}$, J. Electrochem. Soc. 155 (2008) A282.
[34] C. Luo, M. Martin, Stability and defect structure of spinels $Li_{1+x}Mn_{2-x}O_{4-\delta}$, J. Mater. Sci. 42 (2007) 1955–1964.
[35] Y. Gao, J.R. Dahn, The high temperature phase diagram of $Li_{1+x}Mn_{2-x}O_4$ and its implications, J. Electrochem. Soc. 143 (1996) 1783–1788.
[36] J.M. Paulsen, J.R. Dahn, Phase diagram of Li−Mn−O spinel in air, Chem. Mater. 11 (1999) 3065–3079.
[37] C. Dellen, H.-G. Gehrke, S. Möller, C.-L. Tsai, U. Breuer, S. Uhlenbruck, O. Guillon, M. Finsterbusch, M. Bram, Time-of-flight secondary ion mass spectrometry study of lithium intercalation process in $LiCoO_2$ thin film, J. Power Sources 321 (2016) 241–247.
[38] W.A. Ranken, T.W. Bonner, J.H. McCrary, Energy dependence of $^{19}F$ + preactions, Phys. Rev. 109 (1958) 1646–1651.
[39] M. Mayer, SIMNRA, a Simulation Program for the Analysis of NRA, RBS and ERDA, (2016).
[40] A.X.S. Bruker, Topas V4: general profile and structure analysis software for powder diffraction data, Karlsruhe, Germany, J. Electrochem. Soc. 154 (8) (2007) A792–A797.
[41] A. Boulineau, L. Croguennec, C. Delmas, F. Weill, Reinvestigation of $Li_2MnO_3$ structure, Chem. Mater. 21 (2009) 4216–4222.
[42] J. Lee, H. Zhu, G.G. Yadav, J. Caruthers, Y. Wu, Porous ternary complex metal oxide nanoparticles converted from core/shell nanoparticles, Nano Res. 9 (2016)

996–1004.
[43] N. Padmanathan, S. Selladurai, Mesoporous $MnCo_2O_4$ spinel oxide nanostructure synthesized by solvothermal technique for supercapacitor, Ionics 20 (2014) 479–487.
[44] D. Pasero, S. de Souza, N. Reeves, A.R. West, Oxygen content and electrochemical activity of $LiCoMnO_{4-\delta}$, J. Mater. Chem. 15 (2005) 4435–4440.
[45] W. Choi, A. Manthiram, Factors controlling the fluorine content and the electrochemical performance of spinel oxyfluoride cathodes, J. Electrochem. Soc. 154 (2007) A792–A797.
[46] Y.-C. Jin, J.-G. Duh, Fluorination induced the surface segregation of high voltage spinel on lithium-rich layered cathodes for enhanced rate capability in lithium ion batteries, ACS Appl. Mater. Interfaces 8 (2016) 3883–3891.